Simulating the Wave-Enhanced Layer under Breaking Surface Waves with Two-Equation Turbulence Models

HANS BURCHARD

Institut für Meereskunde, Universität Hamburg, Hamburg, Germany

(Manuscript received 8 August 2000, in final form 4 January 2001)

ABSTRACT

The purpose of this paper is to modify two-equation turbulence models such that they are capable of simulating dynamics in the wave-enhanced layer near the surface. A balance of diffusion of turbulent kinetic energy (TKE) and dissipation is assumed as the surface boundary condition for TKE following the suggestion of Craig and Banner. It is shown that this theory, originally developed under the assumption of a macro length scale linearly increasing down from the surface, fails for two-equation models such as the well-known k–ε model. Suggestions are made how to modify such models for overcoming this deficiency. The basic idea is to insert the analytic solution of a model problem suggested by Craig into the dissipation rate equation and solve for the turbulent Schmidt number of the dissipation rate equation, which may be formulated as a function of the production/dissipation ratio. With this modification, the linear behavior of the macro length scale is properly reproduced by the k–ε model. It is shown how near-surface dissipation rate measurements under breaking waves can be simulated by an extended k–ε model considering a shear-dependent closure for the second moments. Finally, the overall performance of this new model approach is tested with a typical upper mixed layer scenario in the northern North Sea.

1. Introduction

With growing computer resources, complex turbulence models have become more and more popular in the field of numerical ocean modeling in recent years. The need for such better models is given by an increasing complexity of problems that have to be solved numerically, ranging from small-scale pollution scenarios in estuaries up to large-scale, long-term global climate change predictions. Improved observation techniques with highly sensitive and fast-responding sensors allow for calibration and validation of new turbulence modeling approaches also under field conditions. In the last decade, enormous progress in the investigation of the dynamics of the upper few decimeters of the ocean has been achieved. After the logarithmic law for profiles of velocity and turbulent quantities near the sea surface had been accepted in the scientific community for a long time, the picture is more precise now. Measurements of various investigators proved the existence of a layer of enhanced (with respect to the log law) turbulence below breaking surface waves (see, e.g., Kitaigorodskii et al. 1983; Thorpe 1984; Osborn et al. 1992). More detailed measurements showed that the turbulent dissipation rate has logarithmic slopes between -2.7 and -1.9 in this wave-enhanced layer, in contrast to -1 for the logarithmic law (see, e.g., Terray et al. 1996; Drennan et al. 1996; Anis and Moum 1995). The present view is that below a near-surface layer of thickness z_0^s in which all properties including the turbulent dissipation rate are well mixed, a wave-enhanced layer with a thickness of about 10 times the so-called surface roughness length is situated. Below that, the ''classical'' law-of-the-wall boundary layer scaling is established. Between these three layers, intermediate states can be found. The wave-enhanced layer is characterized by a shear production orders of magnitude smaller than the turbulent dissipation rate, whereas turbulence production and dissipation are assumed to be of equal size in the log layer below.

In their famous paper, Craig and Banner (1994) suggested modeling the flux of turbulent kinetic energy due to breaking waves into the water column as proportional to the cube of the surface friction velocity. Additionally, they found an analytical solution for an idealized model problem for the wave-enhanced layer by simply neglecting shear production of turbulence. Two years later Craig (1996) published an analytical solution for an idealized model problem that combines both the wave-enhanced layer and the log layer below including the transition zone between both of them. Since then, several authors have included this new approach into their models (see, e.g., Stacey and Pond 1997; D'Alessio et

Corresponding author address: Dr. Hans Burchard, Institut für Meereskunde, Universität Hamburg, Troplowitzstraße 7, Hamburg 22529, Germany.
E-mail: hans@gotm.net

al. 1998; Canuto et al. 2001). These models, however, all have in common that they diagnostically prescribe the macro length scale of turbulence near the surface as proportional to the distance from the surface.

Such an approach is not possible when two-equation turbulence models are used where, besides the turbulent kinetic energy, a prognostic equation for the length scale is calculated. In oceanography, two approaches for such two-equation models are frequently applied, the k–ε model [see Rodi (1980)] and the q^2–q^2l model (Mellor and Yamada 1982). The k–ε model directly calculates the turbulent dissipation rate ε from which the macrolength scale can be derived, whereas the q^2–q^2l model calculates the product of turbulent kinetic energy and the macrolength scale. Both models have often been criticized for their high degree of empiricism (Rodi 1987; Mellor and Yamada 1982), but all alternative, algebraic approaches are based on at least as many empirical assumptions. The advantages of especially the k–ε model are its physical soundness and high numerical robustness as recently shown by Baumert and Peters (2000) and Burchard and Bolding (2001). They are both calibrated such that they reproduce for steady-state constant stress boundary layers the logarithmic law of the wall with a macro length scale proportional to the distance from the surface. It can therefore not be expected that these two models automatically reproduce the correct solutions for the wave-enhanced layer, when only the boundary conditions are properly chosen.

The present paper deals with this problem of generalizing these two-equation turbulence models to the case of a wave-enhanced layer situated above a classical law-of-the-wall layer. For the construction of these modifications, the analytical solution of Craig (1996) is exploited; see sections 2 and 3. This is also used for the formulation of a generalized flux boundary condition for the turbulent dissipation rate ε. The performance of the modified k–ε model is then extensively tested for an idealized model problem; see section 4. Specifically, the numerical discretization is discussed (section 4a), the failure of the unmodified model is shown (section 4b), the sensitivity to numerical resolution is investigated (section 4c), and the performance with higher-order second-moment closures is tested (section 4d). Near-surface dissipation rate measurements, which have been normalized by Terray et al. (1999) are reproduced with the complete modified model (section 5). Finally, the surface mixed layer dynamics in the northern North Sea during four days in spring 1976 are simulated in order to test the capability of the modified model to perform well under highly variable realistic conditions and to demonstrate the potential impact of surface wave breaking on upper mixed layer dynamics (section 6).

2. Analytical solution of the idealized wave-breaking problem

Building up on the Craig and Banner (1994) theory of surface wave breaking assuming a balance of TKE diffusion and dissipation, Craig (1996) suggests an approximate solution for the generalized case of the water column extending from the surface down to the ''law-of-the-wall'' layer under the wave-enhanced layer. In order to construct an idealized model problem for which an exact analytical solution is available, we slightly modify the original model equations.

TABLE 1. Empirical constants for the standard k–ϵ model with surface wave breaking condition.

c_μ	σ_k	c_1	c_2	c_w	κ
0.09	1.0	1.44	1.92	100	0.4

The upward-pointing vertical coordinate z is here constructed such that $z = 0$ is located at the base of the unresolved surface layer (zone of bubble entrainment) with thickness z_0^s. Here, the surface boundary conditions are applied. For simplicity, $z' = -z$ denotes the distance from this upper boundary. In the following, dynamic equations for momentum u and turbulent kinetic energy k are given for a nonstratified water column:

$$\partial_t u - \partial_z(\nu_t \partial_z u) = 0, \tag{1}$$

$$\partial_t k - \partial_z\left(\frac{\nu_t}{\sigma_k}\partial_z k\right) = P - \varepsilon \tag{2}$$

with eddy viscosity

$$\nu_t = c_\mu \frac{k^2}{\varepsilon}, \tag{3}$$

macro length scale

$$L = \kappa(z' + z_0^s), \tag{4}$$

and dissipation rate

$$\varepsilon = (c_\mu^0)^{3/4}\frac{k^{3/2}}{L}. \tag{5}$$

The parameter c_μ, which may be a complex function of mean flow parameters (see section 4d), results from algebraic second-moment turbulence closures. In the standard k–ε model that leads to an analytical solution of the wave-enhanced layer, the so-called stability function c_μ is set to the constant value $c_\mu = c_\mu^0$; see Table 1. In comparison to Craig (1996), the shear production is modified:

$$P = a\frac{(u_s^*)^3}{\kappa(z' + z_0^s)}, \tag{6}$$

where a may be zero or unity, depending on whether wave breaking only is considered (Craig and Banner 1994) or the general case of combining the wave-enhanced and the law-of-the-wall layer (Craig 1996). For $a = 1$, the production for (6) is taken from the analytical solution for the law of the wall without wave breaking. For the full definition of P,

$$P = \nu_t(\partial_z u)^2, \tag{7}$$

an analytical solution could not be found. At the surface the following boundary conditions for momentum,

$$\nu_t \partial_z u = (u_s^*)^2, \qquad z = 0 \tag{8}$$

and turbulent kinetic energy,

$$\frac{\nu_t}{\sigma_k} \partial_z k = c_w (u_s^*)^3, \qquad z = 0. \tag{9}$$

are applied. The latter had been first proposed by Craig and Banner (1994) and models injection of turbulent kinetic energy due to surface wave breaking. The empirical parameter c_w should depend on the wave age and has been estimated to be $c_w = 100$ for fully developed waves. For $c_w = 0$, the classical boundary condition for no wave breaking is retained.

For achieving a problem for which an analytical solution can be found, lower boundary conditions have to be fixed at infinite depth:

$$\nu_t \partial_z u = (u_s^*)^2, \qquad z = -\infty, \tag{10}$$

$$\nu_t \partial_z k = 0, \qquad z = -\infty. \tag{11}$$

For Eqs. (1)–(6) with boundary conditions (8)–(11), the steady-state analytical solution by Craig (1996) is given:

$$k = \frac{(u_s^*)^2}{c_\mu^{1/2}} \left[a + \left(\frac{3\sigma_k}{2} \right)^{1/2} c_\mu^{1/4} c_w \left(\frac{z' + z_0^s}{z_0^s} \right)^{-m} \right]^{2/3} \tag{12}$$

$$\varepsilon = \frac{(u_s^*)^3}{\kappa (z' + z_0^s)} \left[a + \left(\frac{3\sigma_k}{2} \right)^{1/2} c_\mu^{1/4} c_w \left(\frac{z' + z_0^s}{z_0^s} \right)^{-m} \right] \tag{13}$$

with

$$m^2 = \frac{3}{2} \frac{c_\mu^{1/2} \sigma_k}{\kappa^2}. \tag{14}$$

It should be noted that the notation for m deviates from that used by Craig and Banner (1994) and Craig (1996), where $3m$ corresponds to m here. For $a = 0$ and $c_w > 0$, this is identical with the analytical solution presented by Craig and Banner (1994) for $a = 1$ and $c_w = 0$, and the law of the wall is obtained. For the general case, $a = 1$ and $c_w > 0$, the wave-enhanced upper layer and the log layer below can be identified from this solution for k and ε: for $z' \gg z_0^s$, the first term in the brackets, and thus the log law, dominates. For $z' \to 0$, the second term, and thus enhanced turbulence, is dominant, if the standard values in Table 1 are used. With these empirical parameters, a value of $-(m + 1) = -2.68$ results, which is just within the predictions for the logarithmic slope of the turbulent dissipation rate.

3. Modification of the dissipation rate equation

In the well-known k–ε model, the following dynamic equation for the turbulent dissipation rate ε is used (see Rodi 1980):

$$\partial_t \varepsilon - \partial_z \left(\frac{\nu_t}{\sigma_\varepsilon} \partial_z \varepsilon \right) = \frac{\varepsilon}{k} (c_1 P - c_2 \varepsilon), \tag{15}$$

where c_1 and c_2 are empirical parameters (see Table 1). The parameter σ_ε is not independent. Inserting the analytical solution for k and ε, Eqs. (12) and (13), respectively, together with the expressions for ν_t and P, (3) and (6), respectively, into the dissipation rate equation (15) leads for $a = 1$ and $c_w = 0$ to the classical value

$$\sigma_\varepsilon = \sigma_{\varepsilon 1} = \frac{\kappa^2}{c_\mu^{1/2} (c_2 - c_1)} \approx 1.111. \tag{16}$$

This is a well-known result for the logarithmic boundary layer; see for example Rodi (1980) and Burchard et al. (1998).

a. Modification of the turbulent Schmidt number for ε

Also for the ''pure'' wave breaking case with $c_w > 0$ and $a = 0$, an exact value for σ_ε can be found by inserting the analytical solution for k and ε into the dissipation rate equation (15):

$$\sigma_\varepsilon = \sigma_{\varepsilon 0} = \left(\frac{4}{3} m + 1 \right) (m + 1) \frac{\kappa^2}{c_2 c_\mu^{1/2}} \approx 2.4. \tag{17}$$

This is a new result, without which the reproduction of the wave breaking phenomenon with the k–ε model would be inaccurate. However, for the general case, with wave breaking parameterization and consideration of shear production, that is, with $c_w > 0$ and $a = 1$, the derivation of a suitable Schmidt number for the dissipation rate is more problematic since (due to the variation of σ_ε with z) now a complex integral has to be solved. After inserting again the analytical solutions for k and ε into the dissipation rate equation (15) and solving the integral numerically, σ_ε may be described as a function of P/ε, where the cases (16) and (17) are included as $P/\varepsilon = 0$ and $P/\varepsilon = 1$, respectively. In order to obtain this dependency on P/ε, the fact that the expression in the brackets of Eq. (13) equals ε/P with P from Eq. (6) has been exploited. The result is shown in Fig. 1 for $\sigma_k = 1$. It can be seen that the curve for σ_ε is close to a linear interpolation between $P/\varepsilon = 1$ and $P/\varepsilon = 0$.

Equations (16) and (17) could of course also have been used for calculating c_1 or c_2. However, the value for c_2 has been determined as $c_2 \approx 2$ by experiments of freely decaying turbulence behind a grid. The value for c_1, which is more difficult to estimate, has been fixed on dimensional grounds by Tennekes (1989) (see also Baumert and Peters 2000) as $c_1 = 1.5$, a value similar to the one used here (see Table 1). All these considerations assume c_1 and c_2 to be empirical constants. Recently, Canuto et al. (1999) derived new expressions for c_1 and c_2 by analyzing two-point closure models for Reynolds stresses. As a result of that new theory,

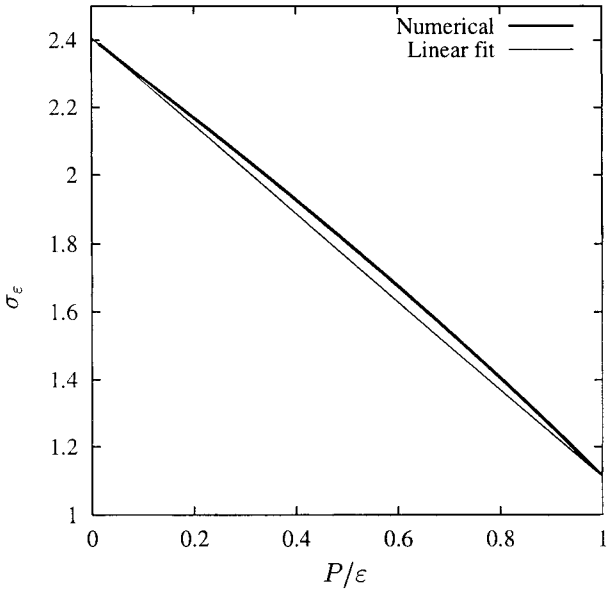

FIG. 1. The Schmidt number σ_ε as it occurs in the dissipation rate equation for $\sigma_k = 1$. Shown are numerical solution of the idealized analytical problem and a linear fit.

$c_2 = 11/6$ is still a constant similar to the empirical value, but c_1 is a function of the invariants of the flow, the turbulent kinetic energy, and the shear production. It will be the task of future investigations to check how such advanced models reproduce dynamics of surface wave breaking. It should be further noted that there are more advanced formulations for the vertical fluxes of turbulent kinetic energy and its dissipation rate. Canuto et al. (1994) derived a complex algebraic closure for the third-order correlators associated with vertical TKE fluxes. The potential of such formulations should be investigated as well.

b. New surface boundary condition for ε

In order to carry out numerical simulations of the wave-enhanced layer with the k–ε model, a surface boundary condition for the dissipation rate ε has to be derived. Burchard and Petersen (1999) have shown recently that the use of flux boundary conditions rather than Dirichlet boundary conditions is advantageous, since (i) the stress-free near-surface dynamics in open channel flow are better reproduced and (ii) the numerical accuracy is much higher. By using the analytical solutions for k and ε, (12) and (13), such a flux boundary condition for ε can be derived:

$$-\frac{\nu_t}{\sigma_\varepsilon}\partial_z\varepsilon = -\frac{\nu_t}{\sigma_\varepsilon}(c_\mu^0)^{3/4}\left\{\left[\frac{3}{2}\frac{\sigma_k(c_\mu^0)^{3/4}}{c_\mu}c_w(u_*^s)^3 + \kappa k^{3/2}\right] \div \kappa^2(z' + z_0^s)^2\right\}. \quad (18)$$

This is a generalization of the flux boundary condition suggested by Burchard and Petersen (1999), which is obtained by setting $c_w = 0$.

4. Idealized numerical simulations

Since indefinite depth is not realizable in a numerical model, a water depth D of 3000 times larger than the roughness length z_0 (here $D = 50$ m and $z_0 = 0.0166$ m^{-s}) is applied for the idealized model simulations. It is assumed that near-bed processes play a negligible role for the wave-enhanced layer. In this section, the standard value for the turbulent Schmidt number for TKE, $\sigma_k = 1$, is used. For all simulations in this paper, the new surface boundary condition for the turbulent dissipation rate, (18), has been applied.

The model is driven with a constant surface friction velocity, which in this case was $u_*^s = 0.01$ m^{-s}. After initializing the velocity with $u = 0$, it took about 5 days of simulation in order to reach a steady-state solution with a constant shear stress over the whole water column.

a. Numerical discretization

For the discretization the water column is divided into N not necessarily equidistant intervals h_i. The grid is staggered, mean flow properties such as velocity or density are positioned in the layer centers, and turbulent quantities such as eddy viscosity ν_t, turbulent kinetic energy k, or turbulent dissipation rate ε are located at the layer interfaces. The vertical diffusion terms are discretized semi-implicitly in time. The sink terms in the equations for turbulent properties such as k and ε are discretized quasi-implicitly in order to guarantee positivity of these quantities also for relatively large time steps.

For the numerical solution, a zooming of layers according to the following formula has been applied:

$$h_i = (\gamma_i - \gamma_{i-1})D, \qquad i = 1, \cdots, N \quad (19)$$

with

$$\gamma_i = \frac{\tanh\left[(d_l + d_u)\dfrac{i}{N} - d_l\right] + \tanh(d_l)}{\tanh(d_l) + \tanh(d_u)} - 1, \qquad i = 0, \cdots, N \quad (20)$$

where D is the height of the water column, N the number of layers, and d_l and d_u zooming parameters. For $d_u = d_l = 0$, the discretization is equidistant, and for $d_l = 0$ and $d_u > 0$, the grid is refined towards the surface. Further details of the numerical discretization can be found in Burchard et al. (1999).

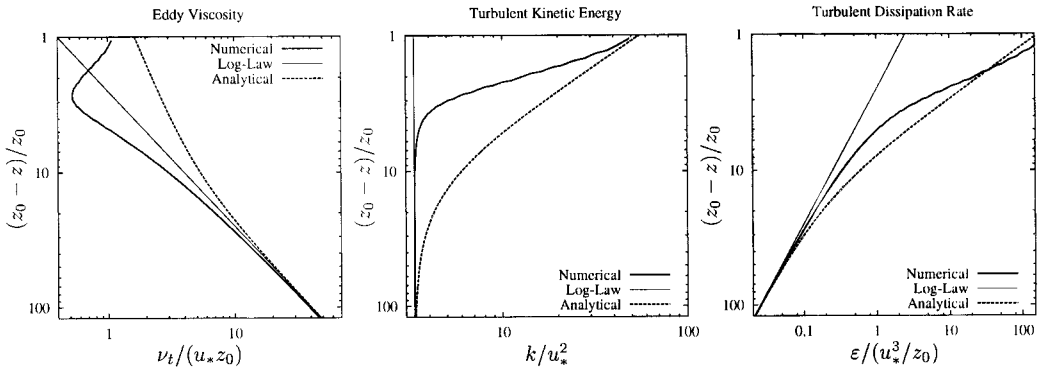

FIG. 2. Results of a numerical simulation of the wave-enhanced layer obtained by the nonmodified k–ε model compared to analytical solutions for the log law and the wave-enhanced layer. Shown are profiles of nondimensional eddy viscosity, turbulent kinetic energy, and turbulent dissipation rate.

b. Simulation results for high numerical resolution

The simulations in this section were carried out with high numerical resolution with $\Delta z/z_0 < 0.1$ at the surface, which was obtained by choosing adequate values for N and d_u with $N = 1000$ and $d_u = 3$.

The need for adapting σ_ε in order to reproduce surface wave breaking is shown in Fig. 2, where the analytical solution is compared to the application of the k–ε model with unmodified turbulent Schmidt number $\sigma_\varepsilon = \sigma_{\varepsilon 1}$ from Eq. (16). It can be seen that the results for k and ε significantly deviate from the analytical solution in the wave-enhanced layer. One might define the depth of the wave-enhanced layer as the depth where the ratio P/ε first deviates less than 1% from unity. This is the case at about $z = -190z_0^s$ for the analytical solution, but at only about $z = -7z_0^s$ for the unmodified k–ε model, which results in a difference of the factor of about 27.

In contrast to that, when using the modified k–ε model, the analytical and the numerical solutions are almost identical if the spatial resolution of the numerical model is sufficiently fine (see section 4a). Small deviations between numerical result and analytical solution are mainly due to the fact that the linear fit to σ_ε has been used instead of the more exact numerical solution (see Fig. 1). Finally, numerical solutions of the complete problem with shear production from (7) instead of (6) are shown in Fig. 3. It should be noted again that an analytical solution for this problem could not be found. It can be clearly seen here that the numerical solution is now sufficiently close to the idealized analytical solution given as Eqs. (12) and (13).

c. Sensitivity to numerical resolution

It would be a desirable property of this model to numerically calculate sufficiently accurate results also for rather coarse vertical resolution. This is important in order to allow for the implementation of this wave-breaking parameterization into three-dimensional models. Here, the same discretization from the previous section is used, changing the zooming parameter d_u such that the ratio $\Delta z/z_0$ varies. Different near-surface resolutions with $\Delta z/z_0 = 0.1, 0.3, 1.0, 3.0$ are tested for which the results are shown in Fig. 4. It seems to be necessary to resolve the surface roughness length with

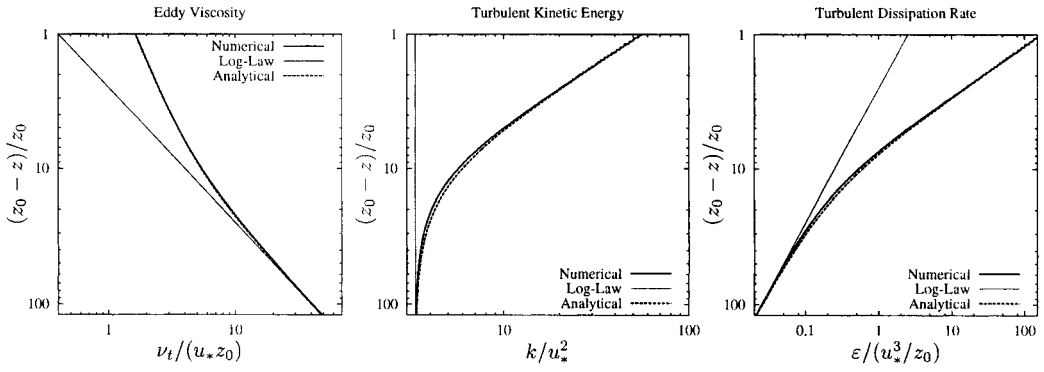

FIG. 3. Results of a numerical simulation of the wave-enhanced layer obtained by the modified k–ε model with constant c_μ compared to analytical solutions for the log law and the wave-enhanced layer. Shown are profiles of nondimensional eddy viscosity, turbulent kinetic energy, and turbulent dissipation rate.

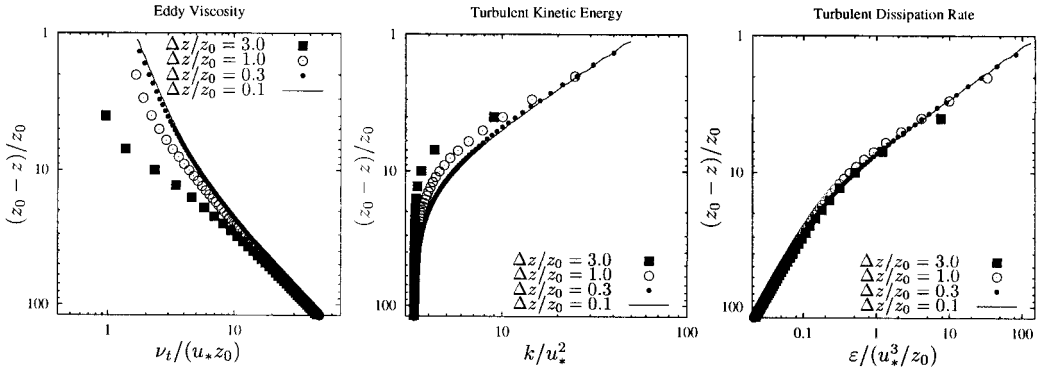

FIG. 4. Results of a numerical simulation of the wave-enhanced layer obtained by the modified k–ε model compared with various vertical resolutions. Shown are profiles of nondimensional eddy viscosity, turbulent kinetic energy, and turbulent dissipation rate.

more than one grid box. With typical roughness lengths of $z_0 \approx 0.2$ m at about wind speeds of around 15 m s^{-1} (see Gemmrich and Farmer 1999), a near-surface vertical resolution of the order of 0.1 m would be needed. This means that estuarine or coastal sea applications can indeed be carried out with this model if surface-fitted coordinates, such as σ coordinates, with zooming toward the surface are used. The high-resolution steady-state simulations presented here could be carried out with time steps of $\Delta t > 200 z_0/u_*$, which would result in time steps up to 1 h for $z_0 \approx 0.2$ m and $u_* \approx 0.01$ m s^{-1}.

d. Shear-dependent stability functions

So far a constant empirical value for the stability function c_μ has been used in order to allow for comparisons with an analytical solution for the turbulence dynamics in the wave-enhanced layer. However, when a proper algebraic second-moment turbulence closure is carried out, this stability function can be expressed as a function of two dimensionless parameters, the shear number and the buoyancy number, respectively:

$$\alpha_M = \frac{k^2}{\varepsilon^2} S^2, \qquad \alpha_N = \frac{k^2}{\varepsilon^2} N^2, \tag{21}$$

where $S^2 = (\partial u)^2 + (\partial v)^2$ is the squared shear frequency (here u is the northward and v the eastward velocity component) and $N^2 = -g/\rho_0 \partial_z \rho$ the Brunt–Väisälä frequency (with density ρ, constant reference density ρ_0, and gravitational acceleration g). Recently, Canuto et al. (2001) suggested such a new set of stability functions, c_μ and c'_μ, which consider more effects of shear and stratification:

$$c_\mu = \frac{0.1070 + 0.01741\alpha_N - 0.00012\alpha_M}{1 + 0.2555\alpha_N + 0.02872\alpha_M + 0.008677\alpha_N^2 + 0.005222\alpha_N\alpha_M - 0.0000337\alpha_M^2},$$
$$c'_\mu = \frac{0.1120 + 0.004519\alpha_N + 0.00088\alpha_M}{1 + 0.2555\alpha_N + 0.02872\alpha_M + 0.008677\alpha_N^2 + 0.005222\alpha_N\alpha_M - 0.0000337\alpha_M^2}. \tag{22}$$

Here c'_μ is used for calculating the eddy diffusivity ν'_t, which is applied for the turbulent mixing of tracers such as temperature and salinity:

$$\nu'_t = c'_\mu \frac{k^2}{\varepsilon}. \tag{23}$$

The dependence of this formulation for c_μ on $P/\varepsilon = c_\mu \alpha_M$ is shown in Fig. 5. For an intensive analysis of these new functions in comparison to others, see Burchard and Bolding (2001).

The simulation of the idealized wave-enhanced layer with this new shear-dependent c_μ shows that the near-surface mixing is further enhanced (see Fig. 6), although the logarithmic slope of the dissipation rate is now slightly smaller than for the constant c_μ. Even if currently no near-surface measurements of turbulence are available that are accurate enough to give preference for one or the other formulation of c_μ, the Canuto et al. (2001) formulation should be applied because of its higher turbulence closure level.

5. Reproducing near-surface dissipation rate measurements

Terray et al. (1999) scaled three different sets of near-surface dissipation rate measurements under breaking

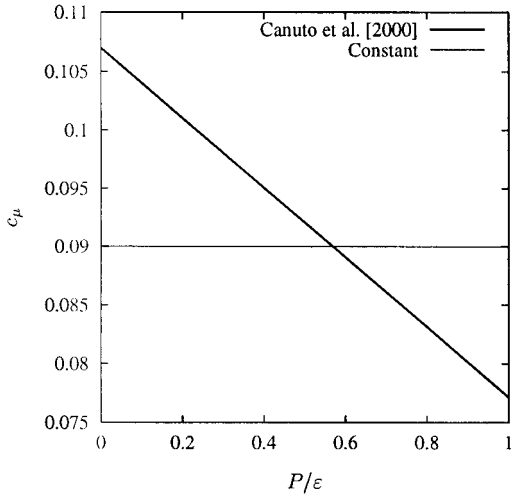

FIG. 5. Stability function c_μ from Canuto et al. (2001) as function of the P/ε ratio in comparison to the standard value for c_μ.

waves such that they more or less collapse into one curve. The scaling of depth was made by using the significant wave height H_s. By comparing the Craig and Banner (1994) model to these data, they found a z_0^s/H_s ratio of 0.85. In Fig. 7, this comparison is reproduced with the k–ε model equipped with the Canuto et al. (2001) shear-dependent stability function c_μ. It can be seen that most of the data fall within the two simulated curves given by $z_0^s/H_s = 0.25$ and $z_0^s/H_s = 1$. It should be noted that recent results of Gemmrich and Farmer (1999) contradict the assumption of a fixed z_0^s/H_s ratio, as there a ratio of less than 0.05 had been measured in the open ocean. Since z_0^s is the significant height of air-bubble entrainment into the water due to wave breaking, it is not necessarily related to the significant wave height. However, in this modeling paper this discussion will not be continued because the surface roughness length is the relevant model parameter that has to be calculated outside the model and then used as model input. It is unfortunately the significant wave height that is part of standard oceanic measurements and not the surface roughness length.

The upper model boundary is here located at the bottom of the unresolved surface layer of height z_0^s, the air-bubble entrainment zone, in which the turbulent dissipation rate is assumed to be constant. At this location, where the vertical coordinate z of the model is set to zero, the macro length of turbulence is fixed to $L = \kappa z_0^s$. This is in accordance to the arguments of Terray et al. (1999) that the length scale should increase proportionally to the distance from the surface. This approach of excluding an unresolved surface layer from the model domain is analogous to the treatment of the bottom boundary layer in many models. In such models, the lower model boundary is located where the extrapolation of the logarithmic velocity is zero. Below that theoretical location the unresolved viscous sublayer is situated.

6. Mixed layer in the northern North Sea

Finally, the ability of the model to perform realistic mixed layer simulations is demonstrated. Near-surface dissipation rate observations over a period of the order of some days are not available yet. Therefore, a classical observational dataset, the so-called FLEX'76 (Fladenground Experiment 1976) from the northern North Sea is reproduced here. A 4-day period in May 1976 will be simulated, which is characterized by a period of weak winds with increasing thermal stratification; a subsequent storm with more than 12 hours duration, which homogenizes the water column down to about 50 m; followed by another weak-wind period. The water depth at the site (58°55′N and 0°32′E) is about 145 m. From April to November a thermocline is established, which separates the surface mixed layer from the bottom mixed layer. Tidal currents with an M_2 amplitude of about 0.2 m s^{-1} create turbulence in the bottom mixed layer due to bottom friction. Here, the dynamics of the whole water column is simulated, but the analysis is focused on the surface mixed layer. For more details about the

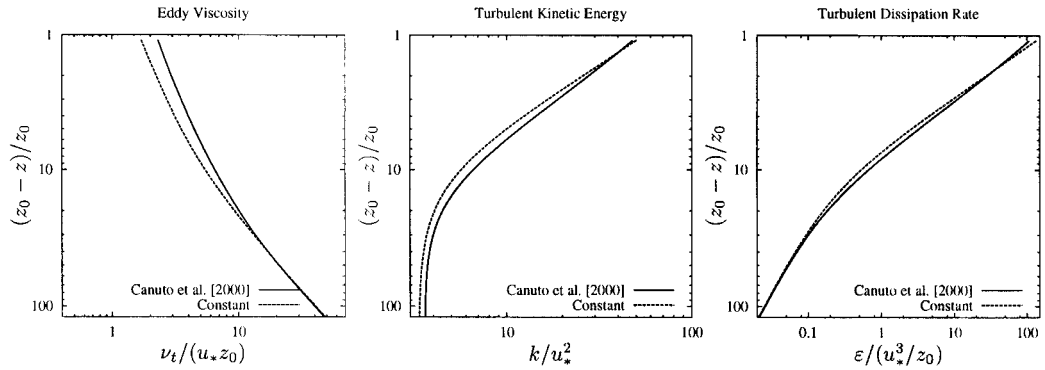

FIG. 6. Results of a numerical simulation of the wave-enhanced layer obtained by the modified k–ε model with constant c_μ and with c_μ from Canuto et al. (2001). Shown are profiles of nondimensional eddy viscosity, turbulent kinetic energy, and turbulent dissipation rate.

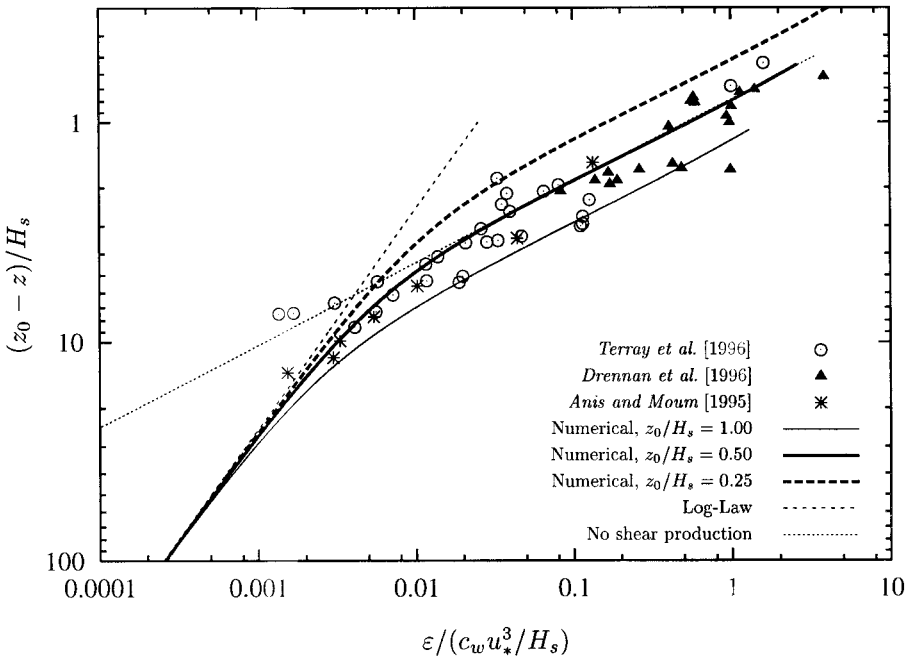

FIG. 7. Observations and simulations of turbulent dissipation rate in the wave-enhanced layer. The observations of Terray at al. (1996), Drennan et al. (1996), and Anis and Moum (1995) are normalized by surface TKE flux and significant wave height (see Terray et al. 1999). The simulations have been carried out with the k–ε model using the modified Schmidt number σ_ε with surface roughness length to wave height ratios of 1, 0.5, and 0.25. The shear-dependent stability function c_μ by Canuto et al. (2001) has been used here. As comparison, the log law with $\sigma_\varepsilon = \sigma_{\varepsilon 1}$ and the pure wave breaking case (no shear production) with $\sigma_\varepsilon = \sigma_{\varepsilon 0}$ are shown as well.

FLEX'76 dataset, see Soetje and Huber (1980) and Burchard et al. (1999) and the references therein.

For this simulation, a set of equations is used of which the equations presented above is a specialization for nonrotational, nonstratified flow. Here, six diagnostic equations for the two velocity components u and v, the temperature T and salinity S, and the turbulent quantities k and ε are calculated. The density ρ is then calculated from T and S by means of the equation of state. All equations are discussed in detail in Burchard and Bolding (2001) and are thus not given here. In addition to the wind forcing, the dynamics of the water column are now driven by surface heat fluxes, solar radiation, and tidally dominated surface slopes. Since now also production and destruction of turbulent energy by stratification are important, the Schmidt number σ_ε for the turbulent dissipation rate ε is a function of the nondimensional parameter $(P + B)/\varepsilon$, where $B = -\nu_t' N^2$ is the buoyancy production of turbulence.

For estimating the sea surface roughness z_0^s, an adaptation of the Charnok (1955) formula to the sea surface is used:

$$z_0^s = \alpha \frac{(u_*^s)^2}{g}, \tag{24}$$

with the dimensionless parameter $\alpha = 1400$ (Craig and Banner 1994). Just to give a feeling for this formula: By using the Kondo (1975) bulk formulae for estimating the air–sea fluxes, under the assumption of no temperature difference between sea and air, a wind speed at 10 m above the sea surface of $U_{10} = 5$ m s^{-1} results in $z_0^s = 0.005$ m and a wind speed of $U_{10} = 25$ m s^{-1} results in $z_0^s = 0.19$ m. This seems to underestimate realistic conditions since Gemmrich and Farmer (1999) measured $z_0^s = 0.2$ at wind speeds of only $U_{10} = 15$ m s^{-1}. Since the aim of this mixed layer simulation is the qualitative investigation of the wave-breaking parameterization inside the k–ε model, a higher value for α will not be used.

The forcing during the four days of simulation and the resulting surface roughness length (which has here been limited by a lower bound of 0.02 m) and simulated sea surface temperature are shown in Fig. 8. The simulated sea surface temperatures, here represented by the value of the uppermost grid box, are nearly identical, with ($c_w = 100$) and without ($c_w = 0$) wave breaking parameterization. This is caused by the fact that the near-surface temperature gradients are weak and therefore do not create increased vertical fluxes due to higher eddy viscosities (see Fig. 9). Therefore it does not matter at which height near the surface the sea surface temperature is defined in order to be compared with the ob-

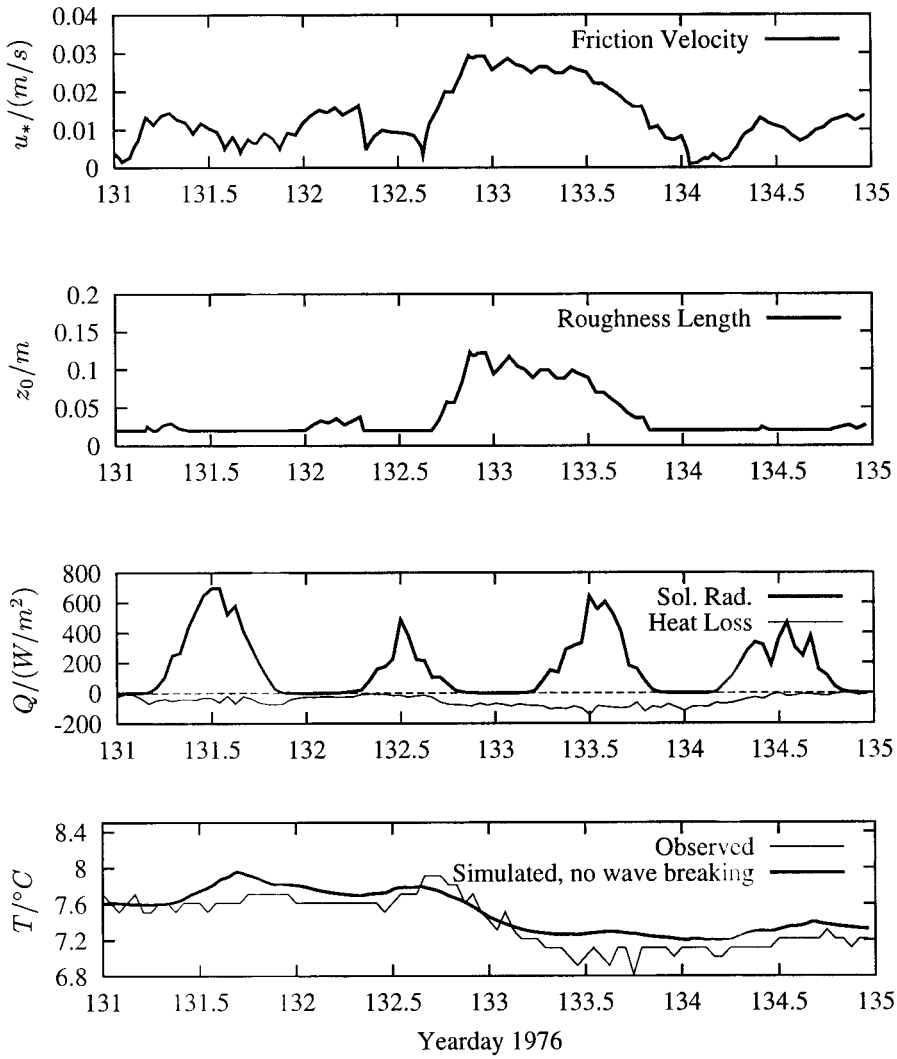

FIG. 8. Time series of surface friction velocity, surface roughness length, solar radiation and surface heat loss, and simulated and observed sea surface temperature before, during, and after a storm at the FLEX'76 central station.

served bulk sea surface temperature. The observations are, in principle, reproduced by the model. Deviations may be explained by wrong estimates of air–sea fluxes, horizontal advection, or inaccurate measurements.

A closer inspection of the simulated current speed profiles before, during, and after the storm (see Fig. 9) reveals that the model indeed predicts a wave-enhanced layer. During the storm this wave-enhanced layer can be clearly seen in the near-surface current speed, which is due to increased vertical mixing significantly smaller with wave breaking parameterization. The vertical mean transport is of course the same with and without wave breaking since the boundary condition for momentum is not affected by the wave breaking parameterization—other than the logarithmic representation of the vertical axis would suggest. In contrast to that, the current speed profiles are hardly affected by wave breaking during calm wind conditions.

For all wind conditions, the wave-enhanced layer can be clearly seen in the profiles of eddy diffusivity, turbulent kinetic energy, and turbulent dissipation rate. The height of the wave-enhanced layer strongly depends on the surface roughness as a function of surface friction velocity. It should be noted that the shape of the turbulent quantities near the surface appear slightly different here in comparison to the previously discussed idealized experiments. This is merely due to the different scaling of the vertical axis. Here, the distance from the lower end of the unresolved surface layer of height z_0^s is shown in contrast to the previous plots where the distance from the surface has been used.

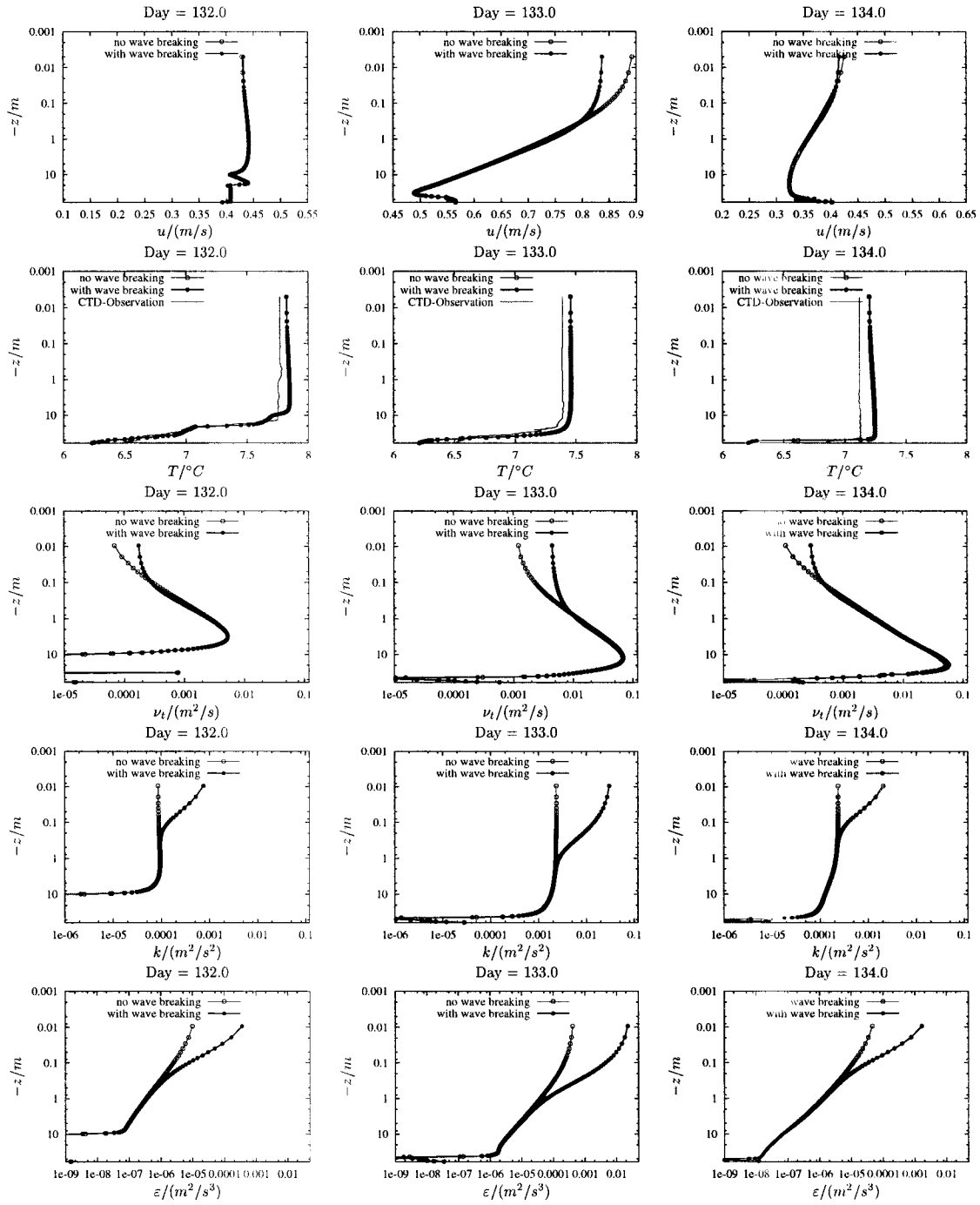

FIG. 9. Profiles of simulated current speed, simulated and observed temperature, and simulated eddy diffusivity, turbulent kinetic energy, and turbulent dissipation rate before (left), during (middle), and after (right) a storm at the FLEX'76 central station. The simulations have been carried out with and without wave breaking parameterization. The vertical axis is logarithmic and for the turbulent quantities the horizontal axis as well.

One interesting feature is that the eddy viscosity after the storm is nearly as big as during the storm. This can be explained with the additional nighttime convective mixing due to the unstable thermal stratification after the storm caused by strong surface heat losses.

It should be noted that a fine vertical resolution near the surface had to be used in order to resolve the wave-enhanced layer also during weak-wind phases with a small surface roughness length. In order to resolve the minimum roughness length of $z_0^s = 0.02$ m, we had to

use $N = 200$ vertical layers with a surface zooming parameter of $d_u = 3.5$. This resulted in a height of the surface layer of less than 0.01 m such that according to the study performed in section 4c a sufficient resolution was reached. In spite of the fine vertical resolution, numerically stable results could be produced with relatively large time steps of $\Delta t = 120$ s.

7. Discussion and conclusions

The well-known k–ε two-equation turbulence model has been modified such that the analytical concept of a wave-enhanced layer located on top of the classical law-of-the-wall layer is reproduced. In order to achieve this, two features of the dissipation rate equation for ε had to be modified: the surface boundary condition and the turbulent Schmidt number σ_ε. Both are derived with the aid of the Craig (1996) analytical approach for this problem and are generalizations of the pure law-of-the-wall situation. For the flux boundary condition a flux proportional to the TKE injection due to breaking waves is added. The turbulent Schmidt number σ_ε is now a function of the turbulence production to dissipation rate ratio and can be closely approximated by a linear interpolation between the law-of-the-wall and the pure wave breaking case.

In contrast to the model with unmodified σ_ε, macro length scales proportional to the distance from the surface could be obtained. This is also the case when the model is extended with a shear-dependent algebraic second-moment closure recently suggested by Canuto et al. (2001). Near-surface dissipation rate measurements could be sufficiently simulated with this extended model. Furthermore, the new model has proven to be numerically stable and could perform a mixed layer simulation over a couple of days. It can therefore be concluded that these modifications to the classical ε equation are reasonable. Without the possibility of adapting the well-tested k–ε model to surface wave breaking, further development of this model would have to be questioned. The method discussed in this paper, inserting the analytical solution of an idealized model problem into the dynamic equations under consideration, could be later applied to more advanced versions of turbulence models, such as the higher-order parameterization of the TKE flux according to Canuto et al. (1994) or the modifications of the empirical parameters in the dissipation rate equation according to Canuto et al. (1999).

The application of modified wave-breaking boundary conditions to two-equation models has already been suggested by others; see Baumert et al. (2000) for the k–ε model. However, the empirical parameters in the length scale–related transport equation have not been adapted in this model. Since they are fitted to represent the law of the wall, which is violated by surface wave breaking, a proper reproduction of the wave-enhanced layer cannot be expected, as shown in section 4b for the k–ε model (see also Fig. 2). The approach presented here could serve as a guideline for how to solve this problem for the q^2l equation in the Mellor and Yamada (1982) two-equation model.

One remaining problem with applying the modified k–ε model to realistic scenarios or three-dimensional models is the need for a near-surface model resolution at least of the order of the surface roughness length. For rather smooth sea surfaces under weak-wind conditions, this could require near-surface layer heights less than 1 cm. For ocean or estuary models with surface-fitted coordinates like the σ transformation this, in principle, should be no problem if vertical mixing processes are discretized implicitly in time [see, e.g., the Princeton Ocean Model by Blumberg and Mellor (1987) or the estuary model by de Kok (1992)]. For numerical models with geopotential coordinates such resolutions are general not realizable due to the free surface elevations [see, e.g., the Modular Ocean Model based on the work of Bryan (1969) and Cox (1984) or the estuary model by Casulli and Cheng (1992)]. It should be noted that such fine resolution near the surface is not needed for the pure log-law case if the boundary conditions are properly discretized (Burchard and Petersen 1999).

There are three quantities connected to the surface wave breaking parameterization, the estimation of which is still a matter of scientific debate: the turbulent Schmidt number for turbulent kinetic energy σ_k, the dimensionless proportionality factor for the amount of TKE injection c_w, and the surface roughness length z_0^s. These quantities are external parameters for the model presented here such that the model will remain valid when changing these values.

The logarithmic slope of the dissipation rate in the wave-enhanced layer is a function of the turbulent Schmidt number for turbulent kinetic energy σ_k. With the standard value of $\sigma_k = 1$, the logarithmic slope is -2.68, which is close to the minimum value suggested by near-surface observations (Terray et al. 1999). The maximum value measured for the logarithmic slope of the dissipation rate in the wave enhanced layer, -1.9, would be obtained by $\sigma_k = 0.29$. Since due to the vanishing flux of TKE in a law-of-the-wall layer the value of σ_k is irrelevant in such situations, there is, in principle, some freedom to adapt σ_k to other observed logarithmic slopes of the turbulent dissipation rate in the wave-enhanced layer. It should be noted, however, that the eddy diffusivity assumption for TKE as well as the existence of a constant turbulent Schmidt number for the TKE are crude model assumptions as well. A full algebraic closure for this term has been suggested by Canuto et al. (1994).

Also, the dimensionless factor for relating the surface TKE flux due to wave breaking, c_w, is subject to debate. Craig and Banner (1994) suggested a constant value of $c_w = 100$, which is used throughout this paper. Other authors prefer to set c_w proportional to the effective wave speed to friction velocity ratio. Terray et al. (1996) sug-

gest such a relationship for young waves only, whereas Gemmrich and Farmer (1999) also use it for well-developed waves. In the latter approach, a fixed effective wave speed of 0.8 m s^{-1} is used in order to account for the fact that this is the wave speed of waves acquiring energy from the wind, which is then transferred to the ocean surface layer. In both approaches, the TKE flux into the water column due to surface wave breaking is proportional to the friction velocity squared in contrast to the original Craig and Banner (1994) approach where it is proportional to the friction velocity cubed.

Finally, the determination of the surface roughness length z_0^s is still an open scientific question. Several authors have related this quantity directly to the significant wave height (e.g., Terray et al. 1996; Drennan et al. 1996; Terray et al. 1999). However, recent field measurements in the open ocean by Gemmrich and Farmer (1999) showed a completely different relation between roughness length and significant wave height, such that obviously more complex parameterizations for the surface roughness length are needed. Stacey (1999) found that the Charnok (1955) formula actually is consistent with a scaling of z_0^s with the significant waves height H_s. Thus, until better parameterizations are found, the Charnok (1955) formula relating surface roughness length to surface friction velocity seems to be a good compromise. The empirical parameter α used within this formula, however, seems to underestimate actual roughness lengths. Craig (1996) concludes that the determination of the surface roughness length will be a major challenge in the future. This is motivated even more after the Gemmrich and Farmer (1999) paper.

It should be noted that the determination of the surface friction velocity itself is a crude estimate, usually made with the aid of bulk formulas. Maybe integrated approaches for the joint modeling of the atmospheric and the oceanic side of the air–sea interface, which resolve the single breaking wave, as recently suggested by Eifer and Donlon (2001) could in the future help to better understand this region of complex dynamics.

Acknowledgments. The work of the author has been funded through a Habilitation grant by the Deutsche Forschungsgemeinschaft (German Research Foundation) and the project PROVESS (MAS3-CT97-0025) of the MAST-III program of the European Commission. All numerical simulations have been carried out with the public domain one-dimensional water column model GOTM (General Ocean Turbulence Model; see http://www.gotm.net). The author is grateful to the coauthors of this model, Karsten Bolding (Ispra, Italy), Manuel Ruiz Villarreal (Santiago de Compostela, Spain), Pierre-Phillipe Mathieu (Reading, U.K.) and Georg Umgiesser (Venice, Italy) for their persistent support. The author is further indebted to Vittorio Canuto (New York, N.Y.), Peter Craig (Hobart, Australia), Walter Eifler (Ispra, Italy), Johannes Gemmrich (Texel, The Netherlands), and Boris Kagan (St. Petersburg, Russia) for their constructive suggestions, and to the participants of the CARTUM concerted action, a turbulence modeling brainstorming project funded in the framework of the MAST-III program of the European Commission (MAS3-CT98-0172), for the interesting and motivating discussions. He is further grateful to two anonymous referees for their constructive comments. They actually both recommended toning down the criticism of the q^2l equation in the Mellor and Yamada (1982) model, for which the author could not find a solution satisfying the analytical solution of the wave-enhanced layer.

REFERENCES

Anis, A., and J. N. Moum, 1995: Surface wave-turbulence interactions: Scaling $\varepsilon(z)$ near the sea surface. *J. Phys. Oceanogr.*, **25,** 2025–2045.

Baumert, H., and H. Peters, 2000: Second-moment closures and length scales for weakly stratified turbulent shear flows. *J. Geophys. Res.*, **105,** 6453–6468.

——, G. Chapalain, H. Smaoui, J. P. McManus, H. Yagi, M. Regener, J. Sündermann, and B. Szilagy, 2000: Modelling and numerical simulation of turbulence, waves and suspended sediments for pre-operational use in coastal seas. *Coastal Eng.*, **41,** 63–93.

Blumberg, A. F., and G. L. Mellor, 1987: A description of a coastal ocean circulation model. *Three Dimensional Coastal Ocean Models*. N. S. Heap, Ed., Coastal and Estuarine Studies, Vol. 4, Amer. Geophys. Union, 1–16.

Bryan, K., 1969: A numerical method for the study of the circulation of the world ocean. *J. Comput. Phys.*, **4,** 347–376.

Burchard, H., and O. Petersen, 1999: Models of turbulence in the marine environment—A comparative study of two-equation turbulence models. *J. Mar. Syst.*, **21,** 29–53.

——, and K. Bolding, 2001: Comparative analysis of four second-moment turbulence closure models for the oceanic mixed layer. *J. Phys. Oceanogr.*, **31,** 1943–1968.

——, O. Petersen, and T. P. Rippeth, 1998: Comparing the performance of the Mellor–Yamada and the k–ε two-equation turbulence models. *J. Geophys. Res.*, **103,** 10 543–10 554.

——, K. Bolding, and M. R. Villarreal, 1999: GOTM—A general ocean turbulence model. Theory, applications and test cases. European Commission Rep. EUR 18745 EN, 103 pp.

Canuto, V. M., F. Minotti, C. Ronchi, M. Ypma, and O. Zeman, 1994: Second-order closure PBL model with new third-order moments: Comparison with LES data. *J. Atmos. Sci.*, **51,** 1605–1618.

——, M. S. Dubovikov, and G. Yu, 1999: A dynamical model for turbulence. IX. Reynolds stresses for shear-driven flows. *Phys. Fluids*, **11,** 678–691.

——, A. Howard, Y. Cheng, and M. S. Dubovikov, 2001: Ocean turbulence I: One-point closure model. Momentum and heat vertical diffusivities. *J. Phys. Oceanogr.*, **31,** 1413–1426.

Casulli, V., and R. T. Cheng, 1992: Semi-implicit finite difference methods for three-dimensional shallow water flow. *Int. J. Numer. Methods Fluids*, **15,** 629–648.

Charnok, H., 1955: Wind stress on a water surface. *Quart. J. Roy. Meteor. Soc.*, **81,** 639–640.

Cox, M. D., 1984: A primitive equation, 3-dimensional model for the ocean. Geophysical Fluid Dynamics Laboratory Ocean Group Tech. Rep. 1, 75 pp.

Craig, P. D., 1996: Velocity profiles and surface roughness under breaking waves. *J. Geophys. Res.*, **101,** 1265–1277.

——, and M. L. Banner, 1994: Modelling wave-enhanced turbulence in the ocean surface layer. *J. Phys. Oceanogr.*, **24,** 2546–2559.

D'Alessio, S. J. D., K. Abdella, and N. A. McFarlane, 1998: A new second-order turbulence closure scheme for modeling the oceanic mixed layer. *J. Phys. Oceanogr.*, **28,** 1624–1641.

de Kok, J. M., 1992: A 3D finite difference model for the computation

of near- and far-field transport of suspended matter near a river mouth. *Cont. Shelf Res.*, **12,** 625–642.

Drennan, W. M., A. A. Donelan, E. A. Terray, and K. B. Katsaros, 1996: Oceanic turbulence dissipation rate measurements in SWADE. *J. Phys. Oceanogr.*, **26,** 808–815.

Eifler, W., and C. J. Donlon, 2001: Modelling the thermal signature of breaking waves. *J. Geophys. Res*., in press.

Gemmrich, J. R., and D. M. Farmer, 1999: Near-surface turbulence and thermal structure in a wind-driven sea. *J. Phys. Oceanogr.*, **29,** 480–499.

Kitaigorodskii, S. A., M. A. Donelan, J. L. Lumley, and E. A. Terray, 1983: Wave turbulence interactions in the upper ocean. Part II: Statistical characteristics of wave and turbulent components of the random velocity field in the marine surface layer. *J. Geophys. Oceanogr.*, **13,** 1988–1999.

Kondo, J., 1975: Air–sea bulk transfer coefficients in diabatic conditions. *Bound.-Layer Meteor.*, **9,** 91–112.

Mellor, G. L., and T. Yamada, 1982: Development of a turbulence closure model for geophysical fluid problems. *Rev. Geophys.*, **20,** 851–875.

Osborn, T., D. M. Farmer, S. Vagle, S. A. Thorpe, and M. Cure, 1992: Measurements of bubble plumes and turbulence from a submarine. *Atmos.–Ocean*, **30,** 419–440.

Rodi, W., 1980: Turbulence models and their application in hydraulics. International Association for Hydraulic Research Rep., Delft, Netherlands, 104 pp.

——, 1987: Examples of calculation methods for flow and mixing in stratified flows. *J. Geophys. Res.*, **92,** 5305–5328.

Soetje, K. C., and K. Huber, 1980: A compilation of data on the thermal stratification at the central station in the northern North Sea during FLEX'76. *''Meteor'' Forschungsergeb.*, **22A,** 69–77.

Stacey, M. W., 1999: Simulation of the wind-forced near-surface circulation in Knight Inlet: A parameterization of the roughness length. *J. Phys. Oceanogr.*, **29,** 1363–1367.

——, and S. Pond, 1997: On the Mellor–Yamada turbulence closure scheme: The surface boundary condition for q^2. *J. Phys. Oceanogr.*, **27,** 2081–2086.

Tennekes, H., 1989: Two- and three-dimensional turbulence. *Lecture Notes on Turbulence*, J. R. Herring and J. McWilliams, Eds., World Scientific, 20–36.

Terray, E. A., M. A. Donelan, Y. C. Agrawal, W. M. Drennan, K. K. Kahma, A. J. Williams III, P. A. Hwang, and S. A. Kitaigorodskii, 1996: Estimates of kinetic energy dissipation under breaking waves. *J. Phys. Oceanogr.*, **26,** 792–807.

——, W. M. Drennan, and M. A. Donelan, 1999: The vertical structure of shear and dissipation in the ocean surface layer. *Proc. Symp. on the Wind-driven Air–Sea Interface-Electromagnetic and Acoustic Sensing, Wave Dynamics and Turbulent Fluxes*, Sydney, Australia, University of New South Wales, 239–245.

Thorpe, S. A., 1984: On the determination of K_v in the near-surface ocean from acoustic measurements of bubbles. *J. Phys. Oceanogr.*, **14,** 855–863.